Ranking uncertainty

Wave climate variability versus model uncertainty in probabilistic assessment of coastline change

Kroon, Anna; de Schipper, Matthieu A.; van Gelder, Pieter H.A.J.M.; Aarninkhof, Stefan G.J.

DOI
10.1016/j.coastaleng.2020.103673

Publication date
2020

Document Version
Accepted author manuscript

Published in
Coastal Engineering

Citation (APA)
Kroon, A., de Schipper, M. A., van Gelder, P. H. A. J. M., & Aarninkhof, S. G. J. (2020). Ranking uncertainty: Wave climate variability versus model uncertainty in probabilistic assessment of coastline change. *Coastal Engineering*, *158*, Article 103673. https://doi.org/10.1016/j.coastaleng.2020.103673

Ranking uncertainty: wave climate variability versus model uncertainty in probabilistic assessment of coastline change

Anna Kroon[a,b], Matthieu de Schipper[a], Pieter van Gelder[c], Stefan Aarninkhof[a]

[a] *Delft University of Technology, Faculty of Civil Engineering, Department of Hydraulic Engineering, Stevinweg 1 Delft, The Netherlands*
[b] *Svašek Hydraulics, Schiehaven 13g, 3024EC Rotterdam, The Netherlands*
[c] *Faculty of Technology, Policy and Management, Department of Values, Technology and Innovation, Section of Safety and Security Science, Jaffalaan 5 Delft, The Netherlands*

Abstract

Sand nourishments are increasingly applied as adaptive coastal protection measures. Predictions of the evolution of these nourishments and their impact on the surrounding coastline contain many uncertainties. The sources that add to this uncertainty can be delineated between intrinsic and epistemic uncertainty, i.e. inevitably in the system or related to knowledge limitations. Effects of intrinsic uncertainty (e.g. due to wave climate variability) on coastal evolution can be significant. In studying these effects, it has often been assumed that intrinsic uncertainty is dominant over epistemic uncertainty (e.g. introduced by the model), yet the magnitude of both contributions have not been explicitly quantified to assess the validity of this assumption. This paper examines the relative importance of intrinsic and epistemic uncertainty in coastline modeling of a large-scale nourishment. It uses a probabilistic framework in which sediment transport is considered to be a function of random wave forcing (intrinsic) and model (epistemic) uncertainty, calculating transport using a one-line model. The test case for this analysis is the mega-nourishment, the Sand Engine, located in the Netherlands. The applied wave climate variability is obtained from long term wave observations, whereas model uncertainty is quantified using

Email address: j.kroon@tudelft.nl (Anna Kroon)

the Generalized Likelihood Uncertainty Estimation (GLUE) method relying on monthly observations. We find that the confidence intervals on predicted volume losses increase substantially when including both intrinsic and epistemic sources of uncertainty. A global sensitivity analysis shows that ignoring model uncertainty would underestimate the variance by at least 50% after a 2.5-year simulation period for the Sand Engine, hence producing significant overconfidence in the results. These findings imply that for coastal modelling purposes a dual approach should be considered, evaluating both epistemic and intrinsic uncertainties.

Keywords: Large-scale nourishment, Model uncertainty, Wave climate variability, Generalized Likelihood Uncertainty Estimation (GLUE), Coastline modeling, Sensitivity Analysis

---

1. Introduction

Coastal sections around the world are increasingly protected with sand nourishments. Yet, using natural dynamics and materials in coastal protection is intrinsically associated with increased uncertainties of the coastal state with respect to more traditional hard protection measures. Recent nourishments along the Dutch coast such as the Sand Engine (de Schipper et al., 2016) and the Hondsbossche Dunes (Kroon et al., 2017) show a significant increase of nourishment volume compared to the more regular beach and foreshore nourishments (Stive et al., 2013). As intervention scales grow and natural variabilities are increasingly incorporated in these designs, the demand for predictions increases, while predictability of the state of the coast at any given time has decreased. In addition to this uncertain response to variable natural forces, many model related uncertainties are present, which are not always included in predicting these coastline changes.

In general, distinction is made between two types of uncertainty, intrinsic and epistemic uncertainty (e.g. Van Gelder, 2000; Van Vuren, 2005). The first is related to the random occurrence of processes in time and space and is irre-

ducible. The second is related to the present state of our process knowledge, models and methods and is in theory reducible given appropriate resources. In Fig. 1 the types of uncertainty in morphological coastline predictions are schematized, adapted from the schematic subdivision of types of uncertainty in design of civil structures by Van Gelder (2000).

In morphological coastline response on a yearly to decadal time-scale intrinsic uncertainty can manifest in both space and time. For instance, the spatial variability in the cross-shore bed levels can have significant influence on the alongshore transport (Mil-Homens, 2016). Likewise, coastal morphology is very sensitive to temporal variability such as the chronology and year to year variability in wave forcing (Southgate, 1995).

Epistemic uncertainty is typically introduced by uncertainties in observations and models. Model uncertainty can be attributed to model inadequacy, parameter uncertainty (e.g. Ruessink, 2005; Simmons et al., 2017) and numerical limitations (e.g. de Vriend, 1987). Model inadequacy can be caused by missing processes (e.g. beach recovery, long waves, sediment sorting; Huisman et al., 2016) or reduced complexity of processes, such as 1D or 2D models and sediment transport formulae. Ruessink and Kuriyama (2008) show that unpredictability of cross-shore sandbar migration during major wave events originates largely from model inadequacy. Parameter uncertainties arise from limited knowledge on actual values of model parameters (e.g. grainsize, bed roughness or wind shear). For instance, Villaret et al. (2016) show that model results are most sensitive to settling velocity and grain size, which are often only locally known. Numerical uncertainties can be introduced by the spatiotemporal model resolution, the order of the numerical schematization and the acceleration technique (Luijendijk et al., 2019). Finally, observation uncertainty is a result of accuracy of the instruments and data processing used. For instance, sampling limitations and measurement errors can significantly contaminate variability at resolved scales, and may lead to errors in the representation of the scales of interest (Plant et al., 2002; Kasprak et al., 2019).

In the last decades, large advances have been made to model and predict

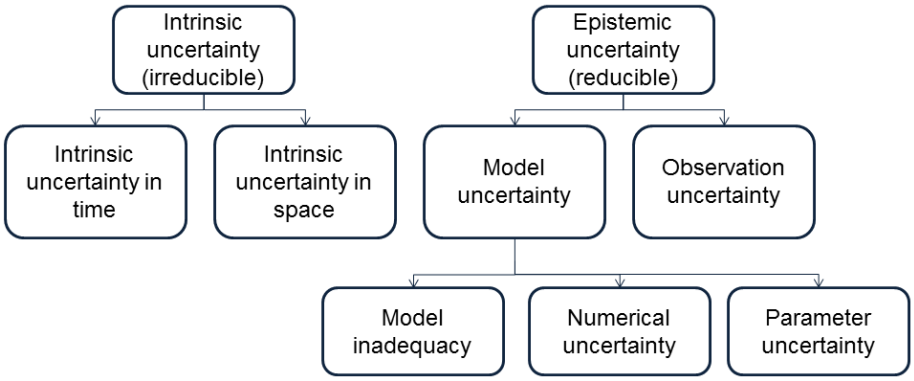

Figure 1: Types of uncertainty in the forecasting of morphological coastline response. Adapted from: Van Gelder (2000)

the morphological processes governing the changes of the coastal zone (Hanson, 1988; Ashton and Murray, 2006; Lesser, 2009; Warner et al., 2010). Thereby making a significant contribution to the accuracy and skill of morphodynamic models, and thus reduction of model uncertainty. However, as focus has been on improvements and strenghts of the model, less detail is presented on the residual uncertainty. Recently, several of these tools have successfully been applied to the modeling of large-scale nourishment evolution (Luijendijk et al., 2017; Arriaga et al., 2017; Tonnon et al., 2018). Although, Arriaga et al. (2017) do acknowledge the sensitivity of the results to different wave climate scenario's, in general, only limited attention is paid to the uncertainties within the predictions.

On a track adjacent to model development and improvement, several of these deterministic models have been applied within probabilistic frameworks to allow for the effects of intrinsic uncertainty (Baquerizo and Losada, 2008; Ruggiero et al., 2010; Ranasinghe et al., 2012; Callaghan et al., 2013; Baart, 2013). The implicit assumptions underlying the focus on intrinsic uncertainty are that climate variability is the most important source of uncertainty and that model

forcing and reliability are independent. That the validity of these assumptions is debatable, is indicated by the results of Callaghan et al. (2013), who show that model uncertainties have a significant influence on probabilistic estimates of storm erosion: the predicted mean erosion and 95% confidence interval vary greatly for each of the models presented and all models overestimate erosion for higher return periods. For the long, climate change time scale, Le Cozannet et al. (2019) show that model uncertainty can indeed be a significant contribution to variance in coastal recession predictions under a rising sea level.

Explicit quantification of model (parameter) uncertainty (epistemic uncertainty) in morphological computations is possible, albeit at a large computational cost (e.g. Kroon et al., 2019; Simmons et al., 2017; Ruessink, 2005). Similarly, it is possible to quantify intrinsic uncertainty in morphological model applications in the coastal zone on a time scale of years (Baquerizo and Losada, 2008; Payo et al., 2008). Yet, combining these to assess the relative importance of epistemic versus intrinsic uncertainty has not been investigated so far.

In coastal engineering the deterministic approach might dominate and probabilistic approaches focus on intrinsic uncertainty, uncertainty analysis in climate change predictions is common practice. In general, three main sources of uncertainty in climate projections are identified: due to future emissions (scenario uncertainty), due to internal climate variability, and due to inter-model differences (IPCC Working Group I, 2013; Hawkins and Sutton, 2011, 2009). Hawkins and Sutton (2011) show clearly that for climate projections the dominant source of uncertainty depends on lead time, climate indicator and spatial scale. Extending these results to coastal morphology, it seems unlikely that intrinsic uncertainty or wave climate variability can be beforehand considered to be the primary source of uncertainty for both short and long time scales. Therefore, this paper includes both intrinsic and epistemic uncertainty in a probabilistic framework to examine the relative importance of these uncertainties in coastline modeling of a large-scale nourishment over time.

For this purpose, sediment transport and volume change are considered to be a function of both intrinsic and epistemic uncertainty. As the principal

source of intrinsic uncertainty we choose the variability in wave climate and as the principal source of epistemic uncertainty we assume model uncertainty. The random wave forcing is based on the observed wave climate variability whereas the distribution of the calibration settings for a simple one-line model are quantified using observations of the Sand Engine nourishment. With a comparison of the observed volume changes and several probabilistic forecasts that include wave climate variability and/or model uncertainty, we show that model uncertainty becomes dominant over wave climate variability for medium-term time scales (years).

2. Sand Engine nourishment

The Sand Engine is a well measured nourishment project, and its large scale results in a distinct and unique coastline response with a high signal to noise ratio. The Sand Engine nourishment was placed between April and June 2011, along the Dutch South Holland coast, as a hook shaped peninsula of 17 million m^3 sand (Stive et al., 2013). The nourishment is exposed to a wind wave climate with a predominant South-West and North-West direction. The spring-neap tidal range varies approximately between 1.5 and 2 m and the local tidal velocities around the peninsula can range up to 1 m/s (Radermacher et al., 2017), but the main driver of the morphological evolution is the alongshore sediment transport by oblique wave incidence (Luijendijk et al., 2017). The bathymetric evolution has been monitored with a 1 to 3 month interval until the end of 2016 and with a 3 to 6 month interval after that (Roest et al., 2017). The grain size (d_{50}) of the Sand Engine varies over the cross-shore profile and in time between approximately 200 and 400 μm (Huisman et al., 2016), and morphological changes can be observed between -8 and 3 m+MSL (de Schipper et al., 2016).

Our analysis starts with the bathymetrical survey of December 2012 because the coastline curvature is too sharp for a one-line model to be stable prior to this date. The remaining 5 year period between December 2012 and January 2018 is

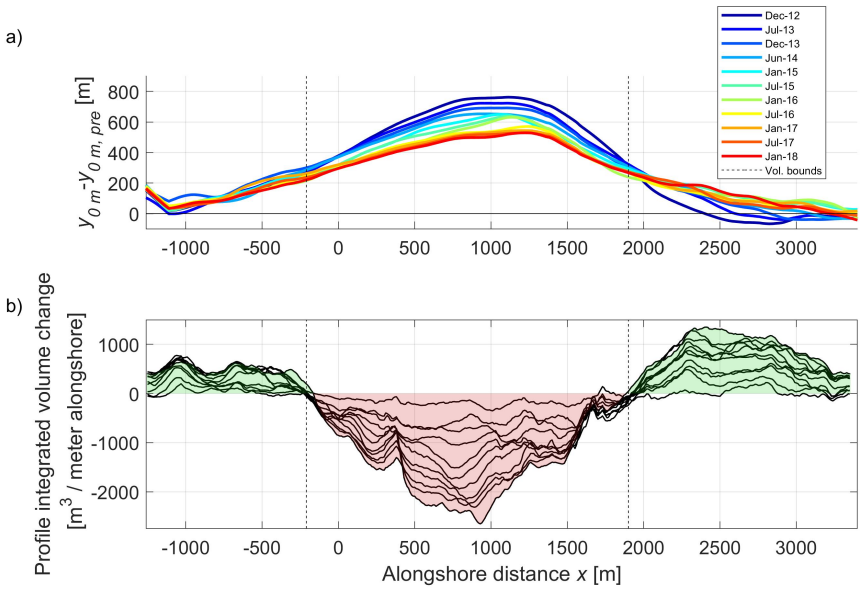

Figure 2: Morphological evolution of the Sand Engine since December 2012. Coastline position, y_{0m}, with respect to a reference coastline, $y_{0m,pre}$, prior to construction of the nourishment (a) and profile integrated volume change since December 2012 (b). The green shaded areas denote net sedimentation and the red shaded area denotes net erosion.

split in two 2.5-year periods: a calibration period and a validation period. The coastline is defined as the position of the most seaward 0 m+MSL depth contour, ignoring the lagoon. The resulting coastline positions since December 2012 are depicted in Fig. 2a. For each of the surveys the profile integrated volume change with respect to the bathymetry of December 2012 is calculated (Fig. 2b). The total volume change (ΔV_{tot}) of the nourishment since December 2012 is calculated as the sum of the net eroding center part of the nourishment (shaded red in Fig. 2b) and shows a negative trend of approximately 500,000 m^3/yr (Fig. 3a). The volume changes between consecutive surveys (ΔV) vary between 100,000 $\pm$ 160,000 m^3 (Fig. 3b). A large volume gain of 8,000 m^3/d, influenced by an observational error, is reported in August 2013. This volume gain is not excluded, exemplifying the effect of measurement errors in the analysis.

To derive model boundary conditions, offshore waves at nearby wave stations

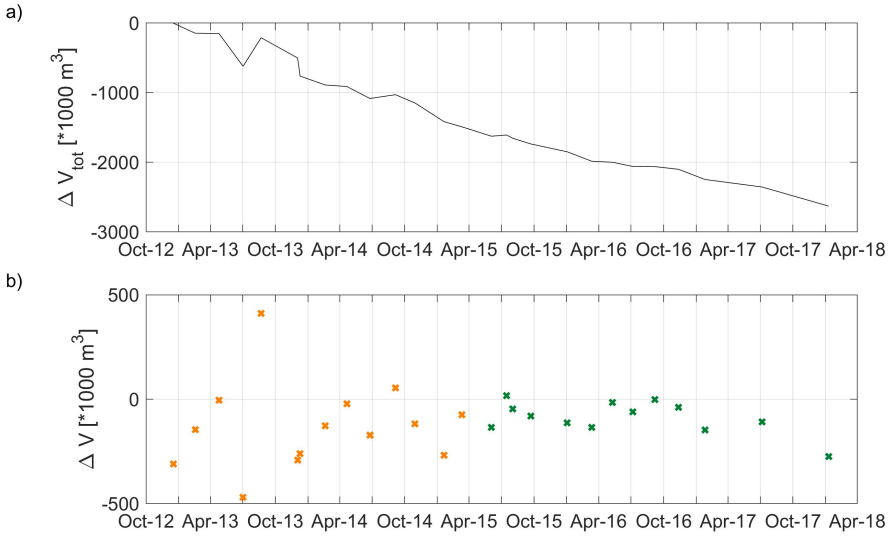

Figure 3: Total volume change (ΔV_{tot}) since December 2012 (a) and volume change (ΔV) between consecutive surveys (b) of the central, net eroding area of the Sand Engine. Orange crosses are used for model calibration and green crosses are used for validation. The positive volume change in August 2013 is influence by measurement errors.

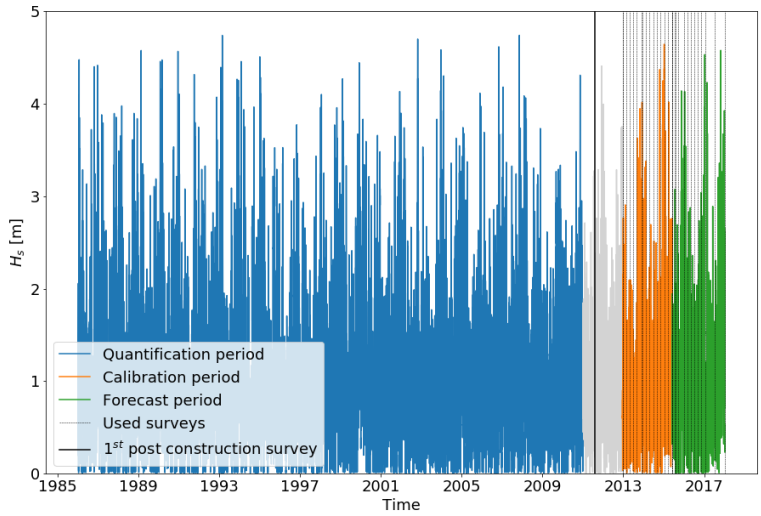

Figure 4: Wave height at the -10 m+MSL depth contour at the Sand Engine for the quantification period (1986-2011), the validation period (December 2012-June 2015) and the forecast period (June 2015-January 2018). Gray dotted lines depict the survey dates. The wave data from January 2011 to December 2012 are not used in the analysis (shown in gray).

are transformed to the -10 m+MSL depth contour with a SWAN model using a transformation matrix derived for the Sand Engine by Deltares (2011) in a similar way to Ly and Hoan (2018). A description of the mesh and a validation for a nearby measurement station can be found in Huisman et al. (2019). The resulting wave height time series (Fig. 4) are separated into three periods: a full 25-year period to quantify the wave climate variability, (January 1986 - January 2011), a 2.5-year calibration period (December 2012- June 2015) and finally a 2.5-year forecasting period (June 2015-January 2018).

3. Methodology

3.1. Probabilistic approach

To examine the relative importance of model uncertainty versus the effects of wave climate variability in predicting coastline change a probabilistic simulation

procedure is followed (Fig. 5). For the morphological computations a one-line model is chosen, to facilitate the large number of computations required to achieve a high statistical accuracy.

The first step in the procedure is to quantify uncertainty. The variation in wave climate is quantified using the statistics of 25 years of wave observations (Fig. 5, left side of blue dotted box). Model uncertainty is quantified using Generalized Likelihood Uncertainty Estimation (GLUE) (Beven and Binley, 1992) that seeks a distribution of appropriate model settings for the 2.5-year calibration period, given a set of observations (Fig. 5, right side of blue dotted box). The next step is to sample from the established distributions of wave climate variability and model uncertainty. So, with a bootstrapping procedure N model time series are generated that meet the observed wave statistics (Fig. 5 left orange box). Whereas N model settings are derived by Monte Carlo sampling (Fig. 5 right orange box) from the derived distribution of model settings. After the deduction of N wave time series and N model calibration factors the uncertainty is propagated trough the one-line model by running it N times for the 2.5-year forecast period (Fig. 5, green box). For each of these runs the volume change in the eroding part of the nourishment is determined, and combining these results provides a probability density function of volume change. We choose $N = 12,000$ samples, this means that we can be 95% sure that the 50% fractile is located between the estimates of the 49% and 51% fractile (Morgan et al., 1990).

In the next part of this section the details of the one-line model and the uncertainty quantification steps are further elaborated upon. Finally, the relative importance of wave climate variability and model uncertainty in this probability density function of volume change is assessed with a global sensitivity analysis (see paragraph 3.5).

3.2. One-line model

Many one-line models can be found in literature with a varying range of complexity (e.g. Arriaga et al., 2017; Payo et al., 2002; WL—Delft Hydraulics,

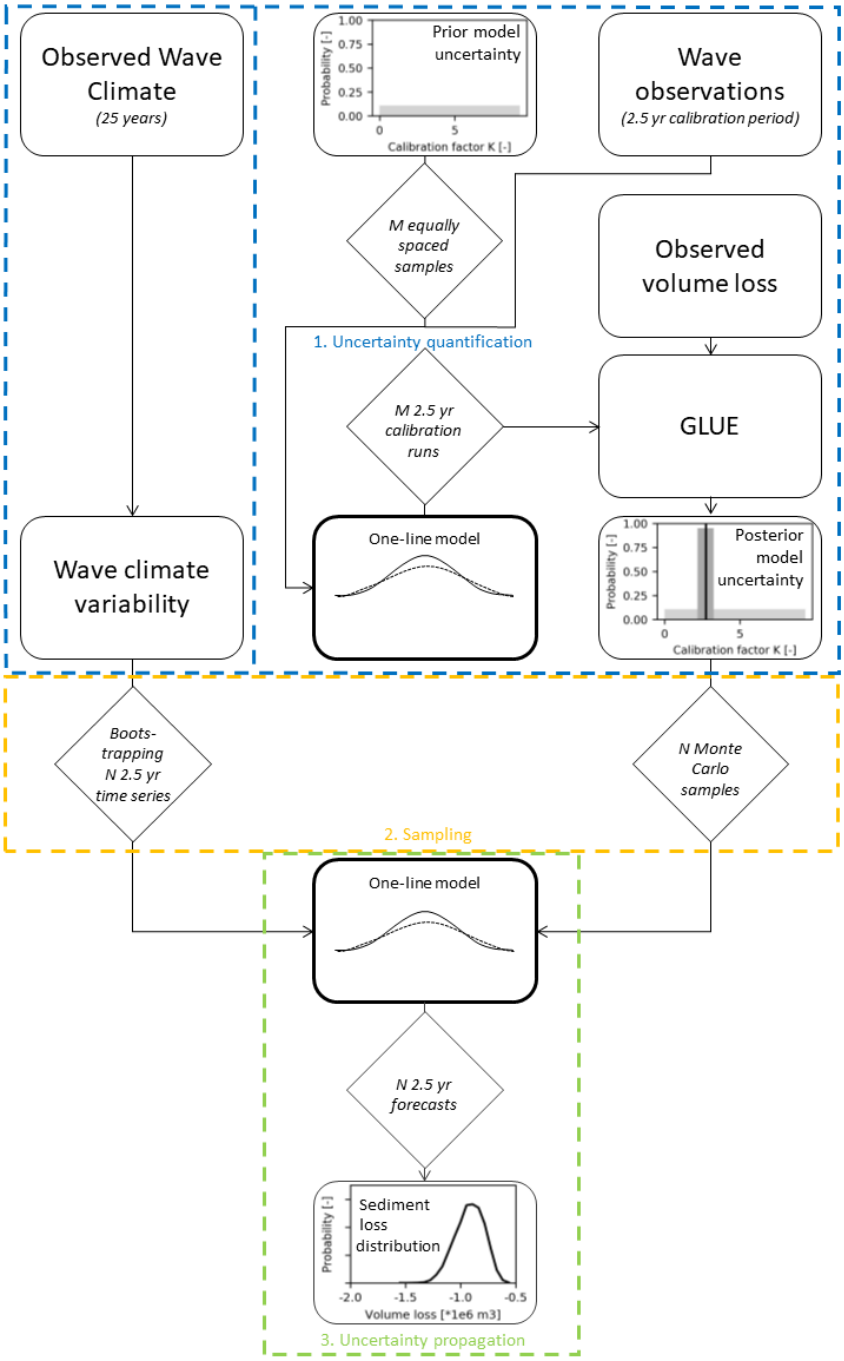

Figure 5: Schematic overview of probabilistic simulation steps: 1) uncertainty quantification, 2) sampling, and 3) uncertainty propagation in a 2.5 yr forecast of volume loss.

1994; Hanson, 1988). In this study a one-line model is used which updates the cross-shore coastline position based on the alongshore sediment transport gradient and neglects any sources or sinks:

$$\frac{\delta y_s}{\delta t} + \frac{1}{D}\frac{\delta Q}{\delta x} = 0 \tag{1}$$

in which x is the alongshore coastline position, y_s is the cross-shore coastline position, Q is the alongshore sediment transport, and D is the active profile height between closure depth and top of the berm. In this approach the alongshore sediment transport rate is calculated with the Kamphuis formula (Kamphuis, 1991):

$$Q = K \tan(\beta)^{0.75} d_{50}^{-0.25} \underbrace{H_{br}^2 T_p^{1.5} \sin^{0.6}(2\theta_{br})}_{\text{wave climate component } (w_{br})} \quad , \tag{2}$$

where Q is expressed as kg immersed mass per second, K is the model calibration factor, $H_{s,br}$, T_p and θ_{br} are the significant wave height, peak period, and angle of wave incidence at the point of breaking relative to shore normal, $\tan(\beta)$ is the beach slope and d_{50} is the median particle size in the surf zone. For the purpose of this study we denote the term that is affected by varying wave forcing as the wave climate component, w_{br}.

To obtain volume change, ΔV_{tot} the coastline change is integrated over the active profile height, D, and the alongshore grid size, Δx, and then summed over the alongshore central section of the nourishment (Fig. 2, dashed lines).

We discretize the coastline of the Sand Engine in non-uniform spaced sections in the x-direction that vary between 200 and 225 m width. H_{br} and θ_{br} are calculated using linear wave theory from waves at a location beyond the closure depth, the -10 m+MSL depth contour. The wave conditions at the -10 m+MSL depth contour are assumed to be constant over the model domain. In addition, we assume d_{50}=300 μm, a beach slope of 1/50 and an active profile height D=11 m. Note that, assuming these specific values may introduce uncertainty in time and space which will be accounted for via calibration of the model calibration factor K as a probability density distribution.

The model calibration factor K as originally proposed by Kamphuis (1991)

has a value of 2.33, assuming a sea water density of $\rho = 1029kg/m^3$. Later, Schoonees and Theron (1996) use an extensive data set to find a value of $K = 3.6$ for exposed sites. In addition, Schoonees and Theron (1996) also reveal significant uncertainty in the exact value of K. The re-calibrated formula still shows deviations from observed transports up to a factor 5 and K values 50% higher or lower only have a marginally higher standard error. Exemplifying that K can be regarded a stochastic variable rather than a deterministic one.

3.3. Quantification of wave climate variability

To force the one-line model with varying wave time-series that follow local wave statistics, the wave climate variability is quantified using available historical wave time series for a 25 year period. This period precedes both the model calibration period and the forecast period (Fig. 4). To maintain seasonal fluctuations and the observed joint probability between H_s, T_p and θ, the time series is separated into monthly sections, providing 25 observations of each month of the year. A bootstrapping procedure (Efron, 1979) is followed to generate a 60-month time series (2.5 years). The forecast time series is built as a sequence of a randomly selected January, followed by a randomly selected February, etc., similar to the method used by Davidson et al. (2017). Using this approach, 25^{60} possible sequences can be constructed. Climate fluctuations such as El Nino and the North Atlantic Oscillation are neglected, meaning that observed extreme months can occur in any year and after any other month. In literature several more elegant, sophisticated but also more complex methods are available to generate synthetic wave time series (e.g. Callaghan et al., 2008; Antolínez et al., 2016; Jäger and Nápoles, 2017). Our forecast period is relatively short and the average wave climate component for both the calibration and the forecast period are comparable to the long term average. Indicating that the wave climate behaves ergodic for the period of our interest, supporting the approach followed.

3.4. Quantification of model uncertainty

The calibration uncertainty is estimated with GLUE (Beven and Binley, 1992; Ruessink, 2005; Simmons et al., 2017) for the 2.5-year calibration period. GLUE was developed as a calibration method which, in contrast to traditional statistical inference, recognizes that the same result can be obtained with different model settings and calls this 'equifinality'. Equifinality is introduced because the model description of the real world is limited and thus contains errors of some extent. Therefore, a parameter set found by calibration can only be assumed to be a likely estimator. GLUE exploits this reasoning by searching within a large parameter space and appointing a non-zero likelihood to all parameter sets that have a prediction skill higher than a certain threshold.

The first step in GLUE is to decide on a likelihood measure and rejection criterion (Beven and Binley, 1992). In this study the Nash-Sutcliffe skill score (Nash and Sutcliffe, 1970) is used which divides the residual variance between model and observation by the variance in the observations as:

$$NS = 1 - \frac{\sum_{i=1}^{n} (dV_i - dV_i')^2}{\sum_{i=1}^{n} (dV_i - d\bar{V})^2} \tag{3}$$

in which dV and dV' are the observed and model predicted volume changes in between surveys, respectively, and n is the number of observations. *NS* is the skill score, a score of one represents a perfect model, whereas a negative score means that the mean square error (MSE) is larger than the observed variance.

In this paper all calibration parameters that result in a prediction with a score higher than zero are included, accepting predictions with a MSE equal or lower than the observed variance. Demanding a positive skill criterion guarantees that our model is behavioral, capturing the overall trend in the observations.

The second step is to decide which model parameters and input variables are considered uncertain. Here, we illustrate model uncertainty with the calibration parameter K.

The third step of the GLUE method is to decide on a prior distribution for

the uncertain parameter(s). In this case we choose a uniform distribution with a wide range, $U(0 - 9.32)$, to minimize subjectivity of the procedure.

Finally, $M = 200$ equally spaced samples of K are drawn from the uniform distribution and used to run the one-line model M times for the 2.5-year calibration period (Fig. 5, right side of blue dotted box), varying the K value for each run while forcing the model with the observed waves of this period (orange line in Fig. 4). The resulting posterior distribution of K will be a uniform distributed PDF but with a reduced range. From this posterior distribution, $N = 12,000$ samples are drawn with a Monte Carlo procedure, and combined with the N synthetic wave time series of 2.5 years to make a probabilistic forecast with the one-line model.

Note that, by assuming K as the only stochastic variable and calibrating to (uncorrected) field observations we do not limit ourselves to parameter uncertainty only, but we include model inadequacies, numerical uncertainties and observation errors in the posterior distribution of K.

3.5. Ranking Uncertainty Sources

The probabilistic procedure results in a distribution of predicted volume change which varies in time. As a first step to achieve the objective of ranking the relative contribution of both uncertainty sources, we perform a local sensitivity analysis in which we compare the magnitude of the variance of the volume change for the wave climate contribution or model uncertainty individually. That means that we pick two locations in the entire range of variables K and w_{br}, the parameter space, at which we compare the variance of ΔV and ΔV_{tot}. We do this for the points with maximum model skill ($Var(Y|K = 2.73)$) and with an average wave climate contribution, $Var(Y|w_{br} = \bar{w}_{br})$ in which $Y = (\Delta V, \Delta V_{tot})$.

The location with maximum model skill and average wave conditions is a point of high interest in the parameter space, but conclusions based on this local comparison are not necessarily true for the entire parameter space. With a global sensitivity analysis (Saltelli et al., 2008) we quantify the fraction of

the variance that can be attributed to a certain input variable for each value in the parameter space. This is described by Sobols' indices which rank the contribution of model uncertainty and wave climate variability to the variance of total volume change. In contrast with a local sensitivity analysis, the global sensitivity analysis takes into account the complete range of the inputs, and attempts to apportion the output uncertainty to the uncertainty in the input factors (Jacques et al., 2006), and this can be done for every output time step. As a result the relative importance can be monitored over time.

The first order Sobol' indices describe the importance of each input variable ($X_i = (w_{br}, K)$) as the contribution of this variable to the total variance of output ΔV_{tot}, and can be calculated with:

$$S_i = \frac{Var(E(\Delta V_{tot}|X_i))}{Var(\Delta V_{tot})} \tag{4}$$

$S_i = 1$ means that all the variance of output variable ΔV_{tot} can be attributed to input variable X_i, contrarily a $S_i = 0$ means that variability in input variable X_i does not translate to variance of ΔV_{tot}. Because our model (Eq. 2) is non-additive, i.e. is a product of two uncertain terms, both uncertainty sources also interact with each other. The interaction term, in case of two uncertain inputs, is given by:

$$S_{12} = \frac{Var(E(\Delta V_{tot}|X_1, X_2))}{\Delta V_{tot}} - S_1 - S_2 \tag{5}$$

3.6. Probabilistic forecasts

Five sets of computations are examined, one calibration set and four different forecasts (Table 1). The calibration set is required to quantify the model uncertainty. The first forecast set includes the quantified distributions of both K and w_{br}. The second forecast includes only the distribution of w_{br} with fixed K as part of the local sensitivity analysis. Similarly, the third forecast includes only the distribution of K with fixed w_{br}. Finally, to examine the effect of a potential dependence between model uncertainty and wave climate variability on the total variance of our prediction, a set of computations is run in which K and w_{br} are correlated with $\rho = 0.5$, according to the findings and procedure of

Description	Calibration	Probabilistic Forecast	Wave climate component only	Model uncertainty only	Correlated Probabilistic Forecast
Run name		$w_{br} + K$	w_{br}	K	$w_{br}\&K$
Number of runs	400	12,000[1]	12,000	12,000	12,000
Period	2012/12 - 2015/06	2015/06 - 2018/01	2015/06 - 2018/01	2015/06 - 2018/01	2015/06 - 2018/01
Wave conditions	Observed 2012/12 - 2015/06	Generated time series	Generated time series	$w_{br} = \bar{w}_{br}$	Generated time series
K	$U(0, 9.32)$	$U(2.18, 3.26)^2$	$K = 2.73^2$	$U(2.18, 3.26)^2$	$U(2.18, 3.26)^2$
Correlation ρ	0	0	0	0	0.5

Table 1: Model settings of different model runs.

Kroon et al. (2019). The marginal distributions of both variables remain equal to the uncorrelated procedure, the only difference is that they are now partially correlated. This means that in case the wave climate component is larger than average in a sample, the probability of a K value larger than average increases.

4. Results

4.1. Uncertainty Quantification

As a first step of the probabilistic assessment, the uncertainty in the wave climate component and the model uncertainty were quantified. The empirical distribution of the wave climate component has a mean of 10 $m^2 s^{1.5}$ and a standard deviation of 19 $m^2 s^{1.5}$ and is highly asymmetrical with a large probability

[1]For the global sensitivity analysis this number of runs is extended to 84,000.

[2]This distribution is the result of the uncertainty quantification procedure, presented in paragraph 4.1.

of lower than average wave climate components. The distribution of the wave climate component (w_{br}) of the generated wave time series perfectly resembles the empirical distribution of $w_{br,obs}$ of the 25 years of observed waves (Fig. 6). The PDF of all generated years (red dashed line) has no bias and deviates only locally (max. 4%) from the long term average observed distribution of w_{br} (black line). Not only the average generated series compare well to the observed series but also more energetic realizations of the wave climate. To exemplify this we compare observed and generated $w_{br,10}$ (green lines). In which $w_{br,10}$ is defined as the generated series or the (consecutive) 2.5-year observation period of which the average has 10% exceedence probability. Compared to the average values (black line), the generated time series with $w_{br,10}$ (green dashed line) has a lower probability of low values ($w_{br}/\overline{w}_{br} < 0.5$) and a higher probability of w_{br} values above average ($w_{br}/\overline{w}_{br} > 1$). This change in distribution is similar to the observed 2.5-year period (green line) with 10% exceedence. This realization of the wave climate with $w_{br,10}$ is also unbiased and deviations are local and limited to 20%. This means that our approach does not only represent the long-term average wave climate component well but also gives a realistic distribution of w_{br} for energetic realizations of the wave climate.

The model uncertainty has been quantified assessing the skill of the 400 calibration computations with random $K \sim U(0 - 9.32)$. A comparison of the predicted and observed volume change between consecutive surveys (ΔV) for the calibration period indicates that the one-line model is able to predict the global observed trend, except for some outliers, Fig. 7. Next, based on the $NS > 0$ criterion, many of the prior calibration values are rejected, resulting in a significantly reduced posterior range of K to $U(2.18, 3.26)$, Fig. 8, while the maximum NS skill is found at $K = 2.73$. The range of K is reduced on both sides of the prior distribution, indicating that the range of the prior was chosen properly.

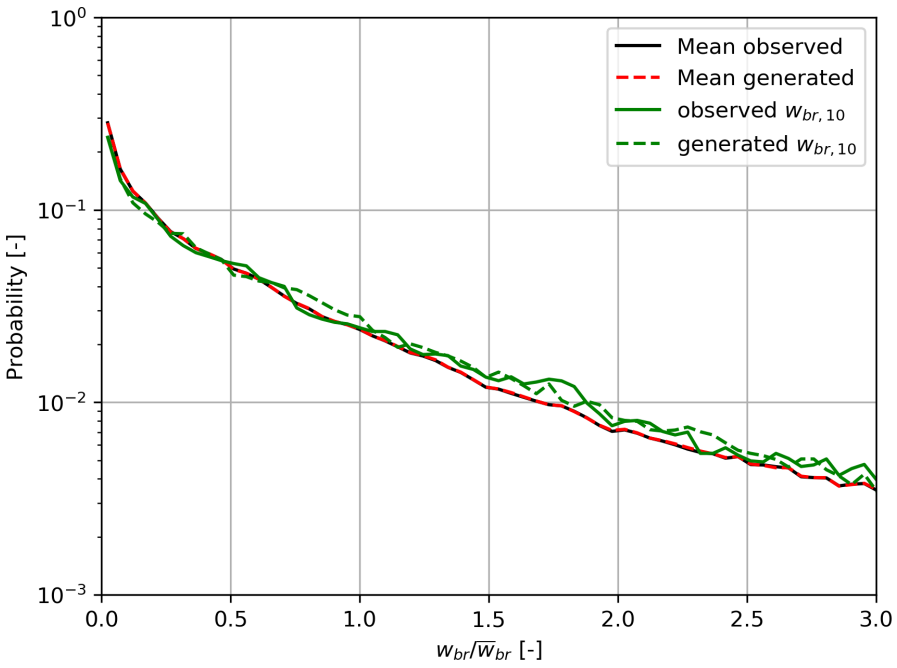

Figure 6: Probability density distribution of normalized wave climate component in Kamphuis formula. Observed (continuous lines) and generated (dashed lines) 2.5-year average (black/red) and 10% exceedence (green).

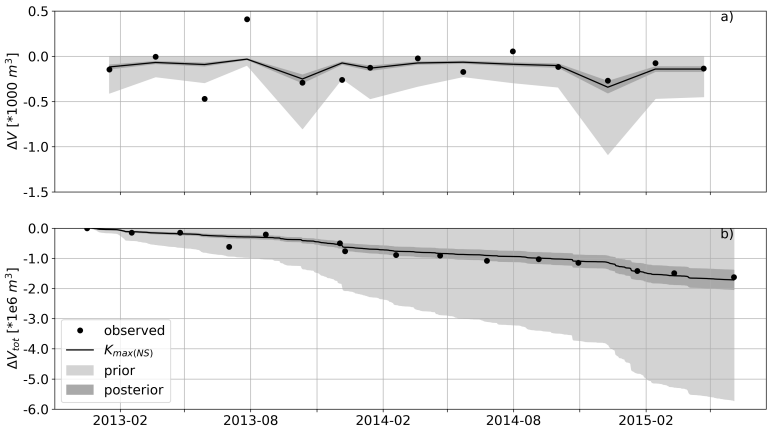

Figure 7: Volume change between consecutive surveys (a) and total volume change since June 2015 (b) for GLUE calibration procedure. The prior distribution (light grey area), the posterior distribution of all runs with $NS > 0$ (dark grey area), and the run with the highest skill score (black line) compared to observed volume change.

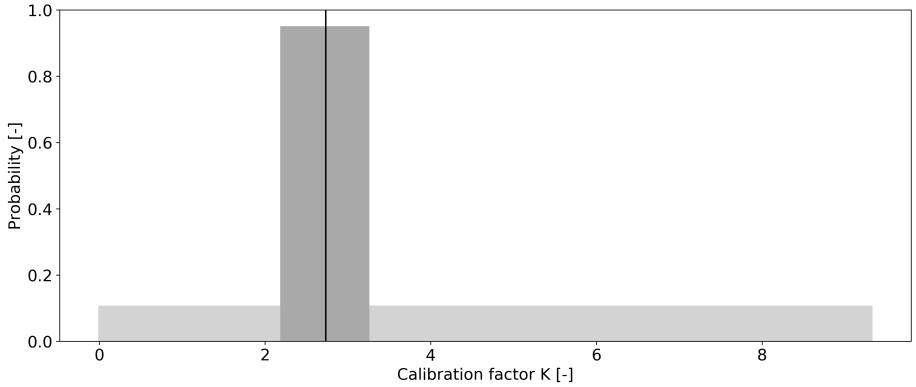

Figure 8: Probability density distribution of model calibration factor K, prior to the GLUE calibration procedure (light grey) and posterior (dark grey). The black line indicates $K = 2.73$, the value with the highest NS skill score.

4.2. Uncertainty propagation

This subsection presents the results of the probabilistic forecasts in which the distributions of K and w_{br}, as derived in the previous section, are propagated through the one-line model to come to a distribution of volume change. Four different forecasts are examined (Table 1). Following the calibration of the model, the adopted model settings are $K \sim U(2.18 - 2.36)$ and w_{br} similar to the empirical distribution of $w_{br,obs}$.

The probabilistic forecast ($w_{br} + K$), predicts a loss of almost 1.000.000 m^3 in 2.5 years with a standard deviation of 15% (Fig. 9b). The observed volume change between consecutive surveys shows a clear summer/winter pattern that is reproduced by the probabilistic forecast (Fig. 9a). The width of the confidence intervals, e.g. the distance between the 5% and the 95% percentile level (Fig. 9a, light grey shade), is a measure for the variance of the distribution. This forecasted variance is higher in winter than in summer. This is an effect of the monthly bootstrapping procedure, which forces the model to have a smaller variance in summer and a larger variance in winter, similar to the observed wave climate. The model bias is negligible, but the variance is much lower than observed. Only 50% of observations fall within the 90% confidence interval, whereas this should be approximately 90%. Similarly only 8% of observed volume changes fall within the 50% confidence interval and no observations fall within the 10% confidence interval (Table 2).

On the other hand, the total volume change is predicted very well by the model (Fig. 9b). The model shows no bias in predicting the total volume change, and the variance of the total volume change is more accurately represented. Hence, 85% of the observations fall within the 90% confidence interval which is very close to the expected 90%. Similarly, 70% and 15% of the observed volume changes fall within the 50 and 10% confidence intervals, respectively (Table 2). The total volume change and the corresponding confidence intervals are predicted remarkably well considering the small number of observations.

Looking at the effects of K and w_{br} individually, we see that the conditional variance of the volume change between consecutive surveys is significantly lower

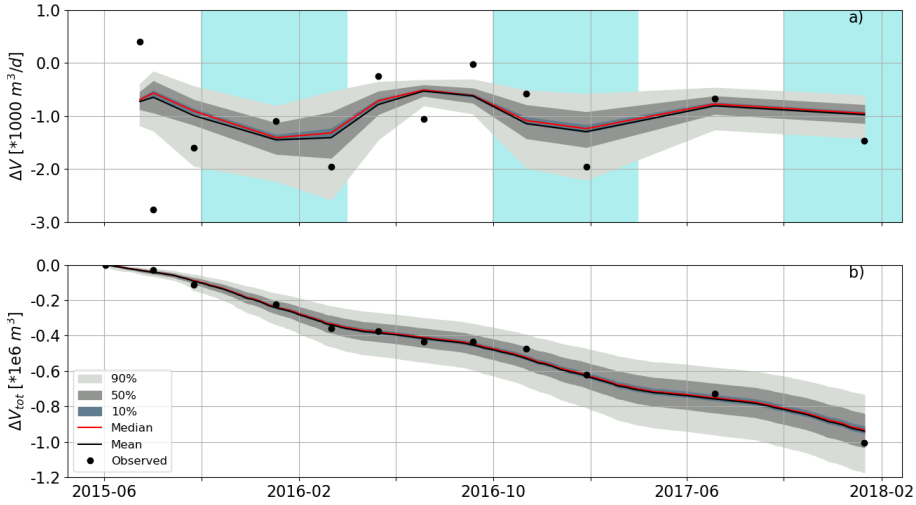

Figure 9: Predicted and observed volume change between consecutive surveys (a) and since June 2015 (b). The mean (red line), median (black line), and the 90, 50 and 10% confidence interval (light gray, dark gray and blue shaded areas) of the probabilistic forecasts are presented together with the observed volume change (black dots). Winter months October to April are indicated with the turquoise background.

when conditioned on the average wave climate component ($Var(\Delta V|w_{br} = \bar{w}_{br})$), than conditioned on the model calibration parameter with the highest skill ($Var(\Delta V|K = 2.73)$) (Fig. 10b and f). However, the variance of the total volume change conditioned on average wave climate component, $V(\Delta V_{tot}|w_{br} = \bar{w}_{br})$, is increasing over time, whereas $V(\Delta V_{tot}|K = 2.73)$ increases initially but becomes stable over time (Fig. 10d and h). As a result, the variance of total volume change conditioned on $K = 2.73$ is ,after 2.5 years (Fig. 10d), approximately equal to the variance of the total volume change conditioned on the average wave climate component (Fig. 10h), meaning that the variance of total volume change is equally sensitive to both inputs at these two locations in the parameter space.

Using Sobol's sensitivity index to quantify this change of relative importance over time globally (Fig. 11), we see that the contribution of K to the total variance of ΔV_{tot} is indeed only 20% at the start of the simulation. However,

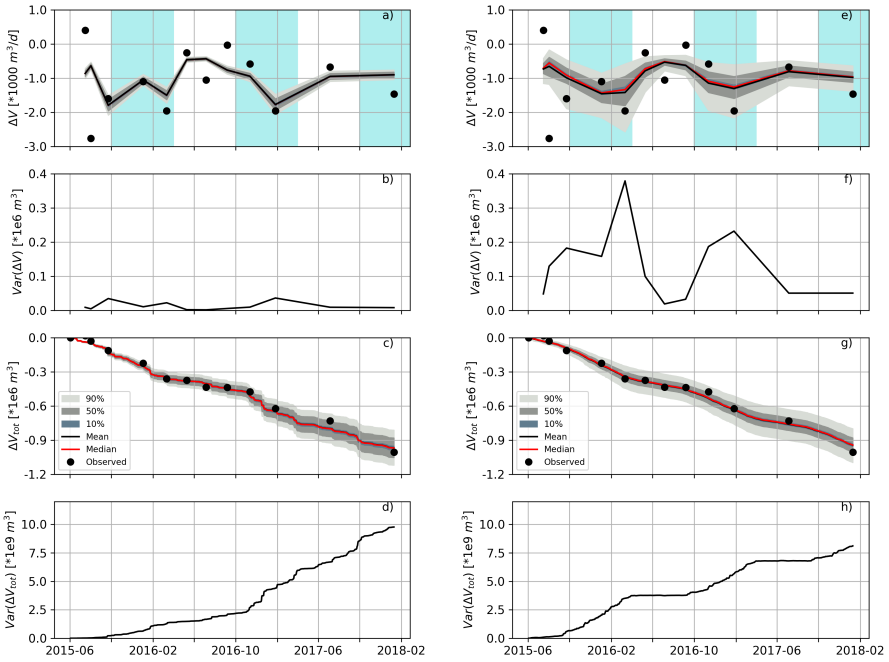

Figure 10: Comparison of predictions with model uncertainty (a-d) and wave climate variability (e-h) only . Predicted and observed volume change between consecutive surveys (a/e), variance of volume change between consecutive surveys (b/f), total volume change since June 2015 (c/g) and variance of total volume change (d/h) . The mean (red line), median (black line), and the 90, 50 and 10% confidence interval (light gray, dark gray and blue shaded areas) of the probabilistic forecasts are presented together with the observed volume change (black dots). Winter months October to April are indicated with the turquoise background.

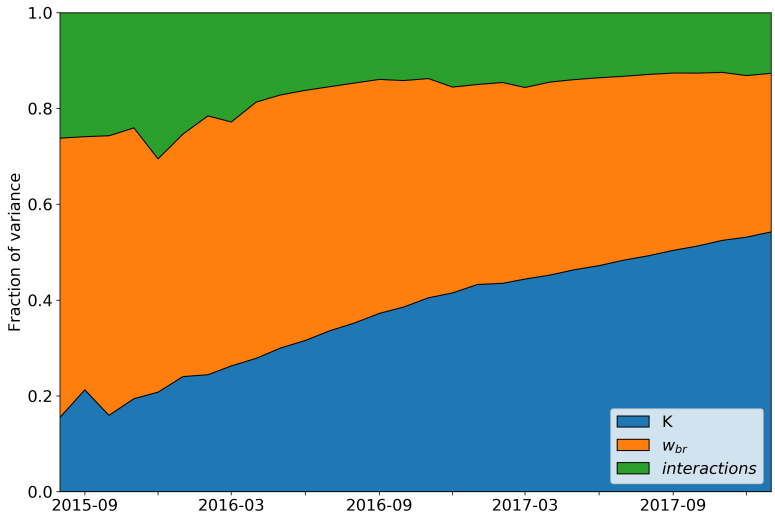

Figure 11: Fraction of the total variance of ΔV_{tot}, of model uncertainty K (blue), wave climate component w_{br} (orange) and interactions between both uncertainty sources (green).

by the end of the simulation this has increased significantly and amounts over 50% of the total variance. w_{br} on the other hand constitutes 60% of the total variance at the start of the simulation but less than 40% after 2.5 years, due to the increasing contribution of model uncertainty to the total variance. In addition, both terms interact explaining another 15-20% of the variance. So, in the case of the sand engine, assessing the effect of wave climate variability only would give a significantly overconfident estimate which neglects more than half the variance.

Sobol's indices cannot be determined for correlated uncertainty sources. Therefore, the effect of a potential correlation between K and w_{br} is assessed by comparing the total variance of the uncorrelated runs (w_{br} and $w_{br} + K$) with the total variance as predicted by the correlated runs ($w_{br}\&K$). Positively correlated uncertainty sources increase the variance of both ΔV and ΔV_{tot}, Fig. 12. Neglecting this correlation results in an additional underestimation of the

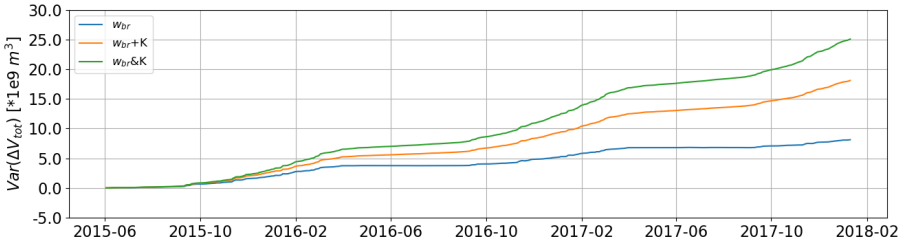

Figure 12: Variance of predicted volume change against time for ΔV (a) and ΔV_{tot} (b).

Confidence interval	ΔV	ΔV_{tot}
90 %	0.50	0.85
50 %	0.08	0.69
10 %	0.0	0.15

Table 2: Fraction of points within confidence interval.

variance by 40% after 2.5 years. So, not attributing for model uncertainty would at least underestimate the variance by 50% in a 2.5-year forecast, but in case of a positive correlation this will be significantly more.

5. Discussion

The probabilistic predictions show that the uncertainty in the volume change at the sand engine nourishment is considerable. We expect a loss of almost 1.000.000 m^3 in 2.5 years with a standard deviation of 15% when including both wave climate variability and model uncertainty. Model uncertainty explains over 50% of the total variance after 2.5 years. These results stress that, for the assessment of large scale nourishments it is not only important to look at variations in wave forcing but also to account for uncertainty in the model(s) used. This conclusion is based on an assessment of a large scale nourishment, yet it is likely that these results are applicable to any sandy solution in the coastal zone.

Evidently, not in all cases the contribution of model uncertainty will be over 50%. For instance, using a more sophisticated model or applying a sandy so-

lution in an environment with a very high variation in wave conditions could reduce the relative importance of model uncertainty. Likewise, predicting a more event driven parameter or process, such as depth of closure, storm retreat or spit breaching, could increase the relative importance of wave climate variability. Also, after the design has been made and a sandy solution has been implemented, the relative importance of model uncertainty in the prediction can in theory be reduced by updating the model uncertainty with new observations once they come available (Vitousek et al., 2017).

Contrarily, the relative importance of model uncertainty will likely increase for smaller nourishments with a less pronounced signal, or in environments with a very narrow distribution in wave forcing (e.g. swell dominated environment). Thus, it is unlikely that in any case model uncertainty (beyond a monthly time scale) can be considered negligible beforehand, without further analysis.

Looking at a slightly longer time scale, the decreasing relative importance of wave climate variability justifies the established use of wave climate reduction in morphological modeling (e.g. Benedet et al., 2016). This is also in line with the findings of Luijendijk et al. (2019), who show that simulations with a reduced wave climate and with brute force time series give a similar prediction of bulk morphometrics such as total volume change after 5 years at the sand engine.

If we extend the time horizon further, other factors, such as sea level rise, can become important contributors to uncertainty. Le Cozannet et al. (2019) use a global sensitivity analysis to show that coastline recession is initially dominated by seasonal, inter-annual and decadal variations, but that the relative importance of model uncertainty increases quickly. Variations in sea level rise scenarios only start to gain importance after half a decade. Although assessing morphological effects of sea level rise, their conclusion is alike: model uncertainty cannot be neglected.

Callaghan et al. (2013) predict beach erosion, a more event driven process, with three different models. The envelope of their multi-model ensemble, is 70-150 % wider than the 95% confidence interval of each model individually. Therewith indicating that in their case, model uncertainties contribute signifi-

cantly to the prediction uncertainty. For comparison, the 95% confidence interval width of our prediction increases with 70% if we include model uncertainty in the analysis.

The underestimation of the observed variance of monthly volume changes (e.g. Fig. 9a) indicates that residual uncertainty remains. Our application of the GLUE method with one free variable, focused on deriving a realistic estimate of model uncertainty, but one can possibly give an improved representation of the observed variance and exploit the full strength of GLUE by assuming more variables to be stochastic. This could be done within the model (e.g. the powers in the Kamphuis formula or the median grain size) but also by including observation uncertainty or adding more processes in the model. So, a straightforward next step is to differentiate between observation and model uncertainty and applying a more advanced model.

In this article, we concentrated on determining the importance of intrinsic versus epistemic uncertainty by distinguishing between wave climate variability and model uncertainty. We found that assessing wave climate uncertainty only, can result in significantly overconfident predictions. Still, in our analysis residual intrinsic and epistemic uncertainty remains, meaning that we might still present an overconfident prediction. Nevertheless, these results clearly show how important it is to be aware of the uncertainties in our models and to be cautious with presenting (un)confidence intervals.

6. Conclusion

This paper includes both intrinsic and epistemic uncertainty in a probabilistic framework, to investigate the relative importance of these uncertainties in the evolution of a sandy solution. To this end, we assess a large scale nourishment case with a one-line model in a probabilistic framework. In this framework, transport and volume loss are considered to be a function of random wave forcing (intrinsic uncertainty) and calibration settings (epistemic uncertainty). The variance of both stochastic variables are based on observations using the Sand

Engine nourishment.

We show that confidence interval width and variance of predicted volume loss increase when allowing for model uncertainty. The confidence interval width and variance increase further (40%) if we not only recognize uncertainty in our model but also include a correlation (of $\rho = 0.5$) between model parameter settings and wave forcing. For the Sand Engine nourishment examined here, the contribution of model uncertainty to the variance of total volume loss is of the same order of magnitude as the contribution of wave climate variability after a 2.5-year simulation period, indicating that accounting for wave climate variability only will produce significant overconfidence in the results. Nevertheless, on a monthly time scale the fraction of variance attributed to wave climate variability is three times larger than that of model uncertainty, thus reducing the importance of model uncertainty in predicting initial nourishment development.

For multi-year time scales, model uncertainty will become the dominant contribution: more wave energy in one year is compensated by less wave energy in another, whereas model uncertainty is a cumulative effect that grows with each time step. Naturally, the relative importance of model uncertainty over wave climate variability depends on the complexity and skill of the model. In general, probabilistic frameworks rely on less complex models to reduce computation time, thereby possibly increasing the relevance of model uncertainty assessment within the framework.

These findings imply that for coastal modelling purposes a dual approach should be considered, evaluating both epistemic and intrinsic uncertainties. Especially when forecasting large scale projects, with simplified models on a multi-year time scale, the uncertainty in model settings may be the principal source of uncertainty.

7. Acknowledgments

The authors want to thank TKI Deltatechnology, the Dutch government Rijkswaterstaat, the water board Hoogheemraadschap Hollands Noorderkwartier,

the contractors Van Oord and Boskalis, and Svašek Hydraulics for their support of this research. Matthieu de Schipper is financed by NWO Domain Applied and Engineering Sciences under project code 15058. Furthermore, a special thanks is given to the two anonymous reviewers, whose comments have made this paper better structured and more readable.

References

Antolínez, J.A.A., Méndez, F.J., Camus, P., Vitousek, S., González, E.M., Ruggiero, P., Barnard, P., 2016. A multiscale climate emulator for longterm morphodynamics (MUSCLE-morpho). Journal of Geophysical Research: Oceans 121, 775–791. doi:10.1002/2015JC011107.

Arriaga, J., Rutten, J., Ribas, F., Falqués, A., Ruessink, G., 2017. Modeling the long-term diffusion and feeding capability of a mega-nourishment. Coastal Engineering 121, 1–13.

Ashton, A.D., Murray, A.B., 2006. High-angle wave instability and emergent shoreline shapes : 1 . Modeling of sand waves , flying spits , and capes. Journal of Geophysical Research 111, 1–19. doi:10.1029/2005JF000422.

Baart, F., 2013. Confidence in Coastal Forecasts. Ph.D. thesis. Delft University of Technology. doi:10.1017/CBO9781107415324.004.

Baquerizo, A., Losada, M.A., 2008. Human interaction with large scale coastal morphological evolution. an assessment of the uncertainty. Coastal Engineering 55, 569–580. doi:10.1016/j.coastaleng.2007.10.004.

Benedet, L., Dobrochinski, J.P., Walstra, D.J., Klein, A.H., Ranasinghe, R., 2016. A morphological modeling study to compare different methods of wave climate schematization and evaluate strategies to reduce erosion losses from a beach nourishment project. Coastal Engineering 112, 69–86. doi:10.1016/j.coastaleng.2016.02.005.

552 Beven, K., Binley, A., 1992. The future of distributed models: Model calibration
553 and uncertainty prediction. Hydrological Processes 6, 279–298. doi:10.1002/
554 hyp.3360060305.

555 Callaghan, D.P., Nielsen, P., Short, A., Ranasinghe, R., 2008. Statistical sim-
556 ulation of wave climate and extreme beach erosion. Coastal Engineering 55,
557 375–390. doi:10.1016/j.coastaleng.2007.12.003.

558 Callaghan, D.P., Ranasinghe, R., Roelvink, D., 2013. Probabilistic estimation
559 of storm erosion using analytical, semi-empirical, and process based storm
560 erosion models. Coastal Engineering 82, 64–75. doi:10.1016/j.coastaleng.
561 2013.08.007.

562 Davidson, M.A., Turner, I.L., Splinter, K.D., Harley, M.D., 2017. Annual pre-
563 diction of shoreline erosion and subsequent recovery. Coastal Engineering 130,
564 14–25. doi:10.1016/j.coastaleng.2017.09.008.

565 Deltares, 2011. Wave look-up table: Building with Nature. Technical Report.
566 Deltares.

567 Efron, B., 1979. Bootstrap methods: Another look at the jackknife. The annals
568 of statistics 7, 1–26. doi:10.1214/aos/1176344552.

569 Hanson, H., 1988. Genesis-A Generalized Shoreline Change Numerical Model.
570 Journal of Coastal Research 5, 1–27.

571 Hawkins, E., Sutton, R., 2009. The potential to narrow uncertainty in regional
572 climate predictions. Bulletin of the American Meteorological Society 19, 1095–
573 1107. doi:10.1175/2009BAMS2607.1.

574 Hawkins, E., Sutton, R., 2011. The potential to narrow uncertainty in pro-
575 jections of regional precipitation change. Climate Dynamics 37, 407–418.
576 doi:10.1007/s00382-010-0810-6.

577 Huisman, B.J.A., de Schipper, M.A., Ruessink, B.G., 2016. Sediment sorting
578 at the Sand Motor at storm and annual time scales. Marine Geology 381,
579 209–226. doi:10.1016/j.margeo.2016.09.005.

Huisman, B.J.A., Walstra, D.J.R., Radermacher, M., Schipper, D.M.A., Ruessink, G.B., 2019. Observations and Modelling of Shoreface Nourishment Behaviour. Journal of Marine Science and Eng. 7. doi:10.3390/jmse7030059.

IPCC Working Group I, 2013. Working Group I Contribution To The IPCC Fifth Assessment Report (AR5), Climate Change 2013: The Physical Science Basis. Chapter 11: Near-term Climate Change: Projections and Predictability. September.

Jacques, J., Lavergne, C., Devictor, N., 2006. Sensitivity analysis in presence of model uncertainty and correlated inputs. Reliability Engineering and System Safety 91, 1126–1134. doi:10.1016/j.ress.2005.11.047.

Jäger, W.S., Nápoles, O.M., 2017. A vine-copula model for time series of significant wave heights and mean zero-crossing periods in the North Sea. Journal of Risk and Uncertainty in Engineering Systems, Part A: Civil Engineering 3, 1–25. doi:10.1061/AJRUA6.0000917.

Kamphuis, J.W., 1991. Alongshore Sediment Transport Rate. Journal of Waterway, Port, Coastal, and Ocean Engineering 117, 624–640. doi:10.1061/(ASCE)0733-950X(1991)117:6(624).

Kasprak, A., Bransky, N.D., Sankey, J.B., Caster, J., Sankey, T.T., 2019. The effects of topographic surveying technique and data resolution on the detection and interpretation of geomorphic change. Geomorphology 333, 1–15. doi:10.1016/j.geomorph.2019.02.020.

Kroon, A., de Schipper, M.A., van Gelder, P.H.A.J.M., Aarninkhof, S.G.J., 2019. Quantification of model uncertainty in lifetime predictions of nourishments, in: Coastal Sediments 2019, pp. 338–346. doi:10.1142/9789811204487_0032.

Kroon, A., de Schipper, M.A., den Heijer, C., Aarninkhof, S.G.J., van Gelder, P.H.A.J.M., 2017. Uncertainty assessment in coastal morphology prediction with a bayesian network, in: Coastal Dynamics Proceedings, pp. 1909–1920.

Le Cozannet, G., Bulteau, T., Castelle, B., Ranasinghe, R., Wöppelmann, G., Rohmer, J., Bernon, N., Idier, D., Louisor, J., Salas-y Mélia, D., 2019. Quantifying uncertainties of sandy shoreline change projections as sea level rises. Scientific Reports 9, 1–11. doi:10.1038/s41598-018-37017-4.

Lesser, G., 2009. An Approach to Medium-term Coastal Morphological Modelling. Ph.D. thesis. Delft University of Technology. URL: http://www.narcis.nl/publication/RecordID/oai:tudelft.nl:uuid:62caa573-4fc0-428e-8768-0aa47ab612a9.

Luijendijk, A., Schipper, M., Ranasinghe, R., 2019. Morphodynamic Acceleration Techniques for Multi-Timescale Predictions of Complex Sandy Interventions. Journal of Marine Science and Engineering 7, 78. doi:10.3390/jmse7030078.

Luijendijk, A.P., Ranasinghe, R., de Schipper, M.A., Huisman, B.A., Swinkels, C.M., Walstra, D.J.R., Stive, M.J.F., 2017. The initial morphological response of the Sand Engine: A process-based modelling study. Coastal Engineering 119, 1–14. doi:10.1016/j.coastaleng.2016.09.005.

Ly, N.T.H., Hoan, N.T., 2018. Determination of Nearshore Wave Climate using a Transformation Matrix from Offshore Wave Data. Journal of Coastal Research 81, 14. doi:10.2112/si81-003.1.

Mil-Homens, J., 2016. Longshore sediment transport bulk formulas and process based models. Ph.D. thesis. Delft University of Technology.

Morgan, M.G., Henrion, M., Small, M.J., 1990. Uncertainty : a guide to dealing with uncertainty in quantitative risk and policy analysis. Cambridge University Press.

Nash, J.E., Sutcliffe, J.V., 1970. River Flow Forecasting Through Conceptual Models Part I-a Discussion of Principles*. Journal of Hydrology 10, 282–290. doi:10.1016/0022-1694(70)90255-6, arXiv:arXiv:1011.1669v3.

Payo, A., Baquerizo, A., Losada, M., 2002. One-line model with time dependent boundary conditions, in: ICCE 2002, pp. 3046–3052. doi:10.1142/9789812791306.

Payo, A., Baquerizo, A., Losada, M.A., 2008. Uncertainty assessment: Application to the shoreline. Journal of Hydraulic Research 46, 96–104. doi:10.1080/00221686.2008.9521944.

Plant, N.G., Holland, K.T., Puleo, J.A., 2002. Analysis of the scale of errors in nearshore bathymetric data. Marine Geology 191, 71–86.

Radermacher, M., de Schipper, M.A., Swinkels, C., MacMahan, J.H., Reniers, A.J.H.M., 2017. Journal of Geophysical Research : Oceans Tidal flow separation at protruding beach nourishments. Journal of Geophysical Research: Oceans 122, 63–79. doi:10.1002/2016JC011942.

Ranasinghe, R., Callaghan, D., Stive, M.J.F., 2012. Estimating coastal recession due to sea level rise: Beyond the Bruun rule. Climatic Change 110, 561–574. doi:10.1007/s10584-011-0107-8.

Roest, L.W.M., De Schipper, M.A., De Vries, S., De Zeeuw, R., 2017. Combined morphology surveys delfland [data set]. doi:doi:10.4121/uuid:d469c50b-edb6-4aa7-811d-f19b389ed344.

Ruessink, B.G., 2005. Predictive uncertainty of a nearshore bed evolution model. Continental Shelf Research 25, 1053–1069. doi:10.1016/j.csr.2004.12.007.

Ruessink, B.G., Kuriyama, Y., 2008. Numerical predictability experiments of cross-shore sandbar migration. Geophysical Research Letters 35, 1–5. doi:10.1029/2007GL032530.

Ruggiero, P., Buijsman, M., Kaminsky, G.M., Gelfenbaum, G., 2010. Modeling the effects of wave climate and sediment supply variability on large-scale shoreline change. Marine Geology 273, 127–140. doi:10.1016/j.margeo.2010.02.008.

Saltelli, A., Ratto, M., Andres, T., Campolongo, F., Cariboni, J., Gatelli, D., Saisana, M., Tarantola, S., 2008. Global Sensitivity Analysis: The Primer. Chichester, UK: John Wiley & Sons.

de Schipper, M.A., de Vries, S., Ruessink, G., de Zeeuw, R.C., Rutten, J., van Gelder-Maas, C., Stive, M.J.F., 2016. Initial spreading of a mega feeder nourishment: Observations of the Sand Engine pilot project. Coastal Engineering 111, 23–38. doi:10.1016/j.coastaleng.2015.10.011.

Schoonees, J.S., Theron, A.K., 1996. Improvement of the most accurate longshore transport formula, in: Coastal Engineering 1996, pp. 3652–3665.

Simmons, J.A., Harley, M.D., Marshall, L.A., Turner, I.L., Splinter, K.D., Cox, R.J., 2017. Calibrating and assessing uncertainty in coastal numerical models. Coastal Engineering 125, 28–41. doi:10.1016/j.coastaleng.2017.04.005.

Southgate, H.N., 1995. The effects of wave chronology on medium and long term coastal morphology. Coastal Engineering 26, 251–270.

Stive, M., de Schipper, M., Luijendijk, A., Ranasinghe, R., van Thiel De Vries, J., Aarninkhof, S., van Gelder-Maas, C., de Vries, S., Henriquez, M., Marx, S., 2013. The Sand Engine: a solution for vulnerable deltas in the 21st century? Coastal Dynamics , 1537–1546.

Tonnon, P.K., Huisman, B.J.A., Stam, G.N., Van Rijn, L.C., 2018. Numerical modelling of erosion rates , life span and maintenance volumes of mega nourishments. Coastal Engineering 131, 51–69. doi:10.1016/j.coastaleng.2017.10.001.

Van Gelder, P.H.A.J.M., 2000. Statistical methods for the risk-based design of civil structures. Ph.D. thesis. Delft University of Technology.

Van Vuren, B.G., 2005. Stochastic modelling of river morphodynamics Stochastisch modelleren van riviermorfodynamica. Ph.D. thesis. Delft University of Technology.

Villaret, C., Kopmann, R., Wyncoll, D., Riehme, J., Merkel, U., Naumann, U., 2016. First-order uncertainty analysis using Algorithmic Differentiation of morphodynamic models. Computers and Geosciences 90, 144–151. doi:10.1016/j.cageo.2015.10.012.

Vitousek, S., Barnard, P.L., Limber, P., Erikson, L., Cole, B., 2017. A model integrating longshore and cross-shore processes for predicting long-term shoreline response to climate change. Journal of Geophysical Research: Earth Surface 122, 782–806. doi:10.1002/2016JF004065.

de Vriend, H., 1987. 2DH Mathematical Modelling of Morphological Evolutions in Shallow Water. Coastal Engineering 11, 1–27.

Warner, J.C., Armstrong, B., He, R., Zambon, J.B., 2010. Development of a Coupled Ocean – Atmosphere – Wave – Sediment Transport (COAWST) Modeling System. Ocean Modelling 35, 230–244. doi:10.1016/j.ocemod.2010.07.010.

WL—Delft Hydraulics, 1994. UNIBEST, A Software Suite for the Simulation of Sediment Transport Processes and Related Morphodynamics of Beach Profiles and Coastline Evolution, Programme Manual. Technical Report. WL—Delft Hydraulics.